Heliyon 9 (2023) e13178

Contents lists available at ScienceDirect

Heliyon

journal homepage: www.cell.com/heliyon

Research article

Gravitational redshift test using Rb clocks of eccentric GPS satellites

Loghman Fathollahi [a], Falin Wu [a,*], Barbara Pongracic [b]

[a] SNARS Laboratory, School of Instrumentation and Optoelectronic Engineering, Beihang University, Beijing, China
[b] iOLAP, Inc., Rijeka, Croatia

ARTICLE INFO

Keywords:
Local position invariance
Gravitational redshift test
GPS
Rb clocks

ABSTRACT

This paper reports a test of gravitational redshift, which is a consequence of the Einstein equivalence principle, using the Rb clocks of GPS Block IIF satellites. The fractional deviation in the gravitational redshift was measured using 6,640 days of data from three Rb clocks onboard GPS Block IIF satellites. The systematic effects related to orbital uncertainty, temperature, and magnetic field were modeled conservatively. The fractional deviation in the gravitational redshift from the general relativity prediction was measured with $(0.23 \pm 1.34) \times 10^{-3}$ at one sigma.

1. Introduction

Gravitational redshift is a consequence of the Einstein equivalence principle (EEP). The EEP includes the independence of the gravitational acceleration of composition (i.e., the weak equivalence principle), independence of the outcome of any local nongravitational test experiment of the velocity of the freely falling reference frame (i.e., local Lorentz invariance), and of the location in spacetime (i.e., local position invariance (LPI)) [1]. The LPI can be tested using typical gravitational redshift experiments, which measure the frequency or wavelength shift $z = \frac{\Delta\nu}{\nu}$ between two indistinguishable frequency standards placed at different heights of a static gravitational field. Based on EEP prediction, the shift for clocks at rest is given by Eq. (1).

$$z = \frac{\Delta U}{c^2}, \tag{1}$$

where ΔU is the difference in the Newtonian gravitational potential between the two clocks, and c is the speed of light. For estimating the magnitude of a possible violation of general relativity, a test of parameter α, which quantifies any deviation from the refined relativistic model, was defined by [2]. The violation of a stationary clock of the relative frequency shift $\frac{\Delta f}{f}$ due to a change in the gravitational potential ΔU is modeled by Eq. (2) [3,4].

$$z = \frac{\Delta f}{f} = (1 + \alpha)\,\frac{\Delta U}{c^2}, \tag{2}$$

with $\alpha = 0$, if the clock rate shows no location dependence.

A series of Pound–Rebka–Snider experiments conducted in 1960–1965 [5,6] provided the first experimental verifications of the gravitational redshift by shift observation using a Mössbauer emitter and absorber at a height difference of approximately 23 m.

* Corresponding author.
E-mail address: falin.wu@buaa.edu.cn (F. Wu).

https://doi.org/10.1016/j.heliyon.2023.e13178
Received 2 October 2022; Received in revised form 27 November 2022; Accepted 19 January 2023

Available online 24 January 2023

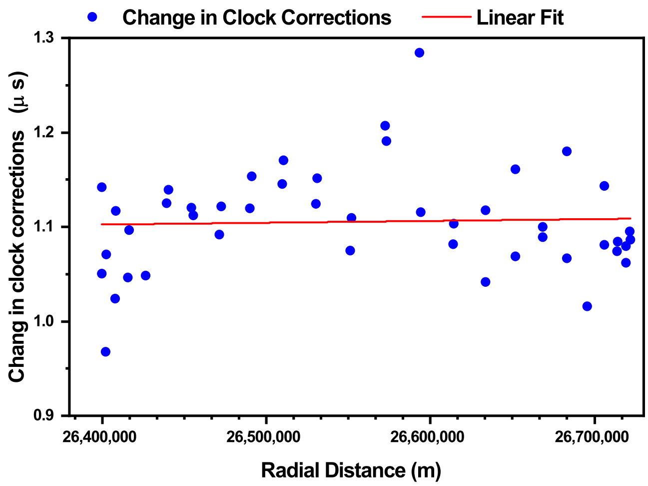

Fig. 1. Changes in the GFZ-published clock corrections every 15 min for PG01 for Modified Julian Day, 57742 (12:00:00 UTC, 20 December 2016), plotted against radial distance.

The most accurate test for gravitational redshift was acquired by the Gravity Probe A (GPA) mission. The GPA mission compared one hydrogen maser on board a sounding rocket launched at a height of 10,000 km above the ground with another corresponding maser on the ground and reached an uncertainty of $|\alpha| \leq 1.4 \times 10^{-4}$ [7–9]. In 2018, using three passive hydrogen maser (PHM) clocks located on two satellites of Europe's Galileo navigation satellite system over data spanning approximately three years, Delva et al. [10] and Herrmann et al. [11] obtained $(0.19 \pm 2.48) \times 10^{-5}$ and $(4.5 \pm 3.1) \times 10^{-5}$ at one sigma for the LPI violation parameter α, which improved the GPA mission test by factors of 5.6 and 4.0, respectively.

Improvements in atomic clock technology have made satellite constellations perfect tools for testing EEP. Some missions have been especially designed for this purpose, such as NASA's Gravity Probe B, the Satellite Test of the Equivalence Principle, and the Micro-Satellite à traînée Compensée pour l'Observation du Principe d'Equivalence. Furthermore, the atomic clocks used in satellites constellations are sensitive enough to test EEP. Our main goal in this study was to investigate GPS atomic clocks for testing gravitational redshift. The first test of LPI using GPS atomic clocks was performed in 2012 [12], where the limit of LPI violation estimated with one year of data from seven stable clocks among 32 operational GPS satellites had a bound of $-0.0027 < \beta_f < 0.0030$. In this study, we tried to improve this method by dealing with systematic errors and improving the statistics model.

2. Materials and methods

In this study, to estimate the LPI violation parameter α, the changes in clock corrections for GPS Block IIF satellites were analyzed. To perform this experiment, accurate measurements of time and position of GPS Block IIF satellites were required. The data can be retrieved from several International Global Navigation Satellite System (GNSS) Service (IGS) analysis centers in the form of Final products, which have the highest quality and internal consistency of all IGS products. The accuracy of the Final products for satellite orbit and the clocks is approximately 2.5 cm and 20 ps [13], respectively. Herein, we used the Final products retrieved from IGS German Research Centre for Geosciences (GFZ) in sp3 format.

The GPS Block IIF series include 12 satellites, which were built by Boeing, launched between 27 May 2010 and 5 February 2016. These satellites were designed for a lifespan of 12 years, and they broadcast multiple improved civilian and military signals (i.e., L1M, L2M, and L2C) and new L5I and L5Q signals. The GPS Block IIF satellites are equipped with two radiation-hardened rubidium atomic clocks and one cesium clock with highly stable timing, and their payloads also include a radiation-hardened 32 bit central processor, and full message encoding and processing techniques. For accurate guidance, control, and navigation, a real-time Kalman filter is applied, and for providing improved crosslink performance, a narrow-band crystal filter is also incorporated [14,15]. The GPS Block IIF Rb AFS clock was built by PerkinElmer, and due to the improved physics package design, its performance is more accurate than that of the GPS IIR Rb AFS [16]. The temperature sensitivity of Rb AFS is less than 5×10^{-14} K^{-1} [17], and the one-day frequency stability of the Rb AFS is $2 \times 10^{-15} \sim 3 \times 10^{-15}$ [18].

2.1. Estimation of α bounds

The procedure proposed by [12] was used to estimate the LPI violation parameter α in this study. The clock correction changes against the radial distance were fitted with linear regression. Fig. 1 shows an example of these fits. All nonzero slopes of the fits were used to estimate conservatively large bounds for LPI violation, which were attributed to α, as defined by Eq. (3).

$$\alpha = m \frac{r_a - r_p}{2\Delta T_{\max}}, \tag{3}$$

where r_a is the radius at apogee, r_p is the radius at perigee, m is the slope of the linear fit of clock correction changes against the radial distance, and $\Delta T_{\max}$ is the maximum theoretical clock correction of a satellite at apogee, as defined by Eq. (4) [19].

$$\Delta T_{\max} = \frac{T_{\text{ep}}\left(\left(\Phi_a - \frac{v_a^2}{2}\right) - \left(\Phi_i - \frac{v_i^2}{2}\right)\right)}{c^2}, \tag{4}$$

where Φ_a and v_a are the gravitational potential per unit mass and the velocity of a satellite at apogee, respectively; Φ_i and v_i are the gravitational potential per unit mass and the velocity of a satellite in an ideal circular orbit for GPS orbit, respectively; T_{ep} is the period between two epochs, which is 15 min.

The best-fit slope and corresponding α values were calculated for the selected satellites for the revolution of each satellite around the Earth. The annual oscillations are likely caused by atmospheric effects [12]. The annual oscillations and short-term fluctuations were estimated from the calculated value of α. The short-term fluctuations were filtered out using a moving average. For removing the annual oscillation, a least-squares fit as given by Eq. (5) was implemented.

$$y = A + B\cos\left(\frac{2\pi t}{T_d} + \varphi\right), \tag{5}$$

where A, B, and φ are the fit parameters; T_d is the time period of the data; and then $B\cos\left(\frac{2\pi t}{T_d} + \varphi\right)$ was subtracted from daily values.

2.2. Systematic effect modeling

As presented by references [10,11,20], systematic effects are mainly caused by magnetic field, temperature effect, and satellite orbital modeling error.

Magnetic field correction: As proposed by Angelopoulos et al. (2008) [21] and Tsyganenko (2007) [22], the clock's magnetic sensitivity and the International Geomagnetic Reference Field model [23] were employed to model the magnetic field effect at GPS altitude in this study. To estimate the uncertainty of the magnetic field, the total magnetic field effect was considered instead of its projection onto a specific Rb clock's axis. The relative frequency for the Rb clocks was smaller than 1×10^{-13} G^{-1} [17]; this sensitivity was applied to the clock firstly, and then the model was used to translate the magnetic field variations in the local frame axis into a maximum fractional frequency variation in the atomic clock in orbit. The total uncertainty of the magnetic field was estimated as the differences of α_+ and α_-, where α_+ and α_- are for add and subtract correction, respectively.

Temperature effect correction: Temperature is controlled by thermal pipes in the clock location, and we modeled the maximum possible temperature variation with a focus on satellite orientation. The temperature variation ranges for the Rb clocks in GPS IIR/IIR-M are ± 2.25 K [24] and, the observed maximum peak-to-peak variation for GPS satellites is 0.5 K [16]. This temperature variation was attributed to the orbital period. The ground temperature sensitivity range in the relative frequency for the Rb clocks was established as $< 5 \times 10^{-14}$ °C [17]. In this study, the clock variation was attributed to the satellite's orientation change with respect to the Sun. In addition, the thermal control system allowed us to record their range variation in the form of peak-to-peak variation.

Orbital modeling correction: The force from the solar radiation pressure (SRP) is the largest perturbation acting upon GNSS satellites after the gravitational attraction from the Earth, Sun, and Moon, which makes it the largest source of error in the modeling of GNSS orbital dynamics. The clock error is attributed to the radial part of orbit error, and the angle between the satellite orbital plane and the direction of the Sun (i.e., Sun elevation angle β). The satellite laser ranging (SLR) residuals correlated to the clock offset and radial orbit error can be considered as a measure of the radial orbit error [25]. Unfortunately, no SLR data are available for correcting GPS orbit; in this study, we considered that the orbital systematic effects depend on the Sun direction as well as the mean anomaly of GPS satellite. The enhanced SRP model for GPS satellites proposed by [26] was used to model the orbital uncertainty caused by SRP. A good fit between the observed variation and a function of β angle is given by Eq. (6) [26].

$$F(\beta) = A + B\sin\beta + C/\sin\beta + D\cos\beta, \tag{6}$$

where A, B, C, and D are separate empirical parameters describing the C_Y_1, S_X_2 shape factor to combine SRP equations for the GPS solar radiation pressure model (GSPM) (see Table 5 in [26]), and box-wing parameters can be found in Table 4 in [26]. These two sets of parameters were estimated with six years of GPS measurements. The physical effects, including yaw bias, radiator emission in the satellite body-fixed $-X$ and Y directions, and the thermal radiation of solar panels, were considered as additional constant parameters in the optical parameter adjustment [26].

All systematic effects contributing to the final error budget are summarized in Table 1. The systematic corrections and their uncertainties were combined using a quadratic sum of the individual uncertainties. The final mean value of error and its uncertainty with an equal-tailed 68% confidence interval for each clock were derived from the different systematic corrections, as shown in Fig. 4.

2.3. Relativistic effect

Second-order relativistic correction for nonzero orbit ellipticity $-(2r \cdot v)/c^2$ is routinely applied by GFZ [27], but as shown in [28], this correction leads to two types of error: a missing relativistic effect because of the oblateness of the Earth, as well as

Table 1
Error budget of statistical corrections and systematic uncertainties. All errors are in the 1σ interval. Statistical error estimated from distribution of fit results. Systematic uncertainties for magnetic fields and temperature are upper and lower bounds (assuming uniform distribution).

Groups	LPI violation $\times 10^{-3}$	Total $\times 10^{-3}$	Stat $\times 10^{-3}$	Orbit $\times 10^{-4}$	Temp $\times 10^{-5}$	Mag $\times 10^{-5}$
PG01	0.49	1.85	1.83	2.65	0.76	0.77
PG10	0.14	1.67	1.65	2.66	1.11	1.12
PG30	0.17	1.26	1.23	2.65	0.86	0.85
Combined	0.23	1.34	1.31	2.65	2.54	2.52

Table 2
Details of GPS Block IIF satellites. PRN, pseudo-random noise.

PRN	Satellite Clk	Lunch Date (UTC)	Launch Vehicle	Clk Corr SD (ms)	Days Included
PG01	Rb	2011/07/16	Delta IV	**101.8**	2,310
PG03	Rb	2014/10/29	Atlas V	161.0	-
PG06	Rb	2014/05/17	Delta IV	200.5	-
PG09	Rb	2014/08/02	Atlas V	248.2	-
PG10	Rb	2015/10/31	Atlas V	**150.3**	2080
PG25	Rb	2010/05/28	Delta IV	270.5	-
PG26	Rb	2015/03/25	Delta IV	243.6	-
PG27	Rb	2013/05/15	Atlas V	185.9	-
PG30	Rb	2014/02/21	Delta IV	**112.3**	2250
PG32	Rb	2016/02/05	Atlas V	242.8	-

non-Keplerian perturbations. Both of these effects are not considered in the Keplerian model. The full relativistic model is given by Eq. (7) [19,28,29].

$$\Delta t^{\text{rel}} = \left[S^{\text{offset}} + \delta\Delta t^{\text{con}}(a_0)\right] t + \Delta t^{\text{per}} + \delta\Delta t^{\text{rel}}, \tag{7}$$

where t is the satellite time observed on the ground, S^{offset} is the nominal frequency offset, Δt^{per} is the conventional satellite relativity correction, as given by Eq. (8).

$$\Delta t^{\text{per}} = -\frac{2r \cdot v}{c^2}, \tag{8}$$

where r and v are the radius and velocity vectors of the satellite, respectively. $\delta\Delta t^{\text{con}}(a_0)$ is the relativistic time correction caused by the departure of the mean semimajor axis (a_0) from the nominal satellite semimajor (a_n), and $\delta\Delta t^{\text{rel}}$ is the desired approximate correction with respect to the conventional satellite relativity correction (Δt^{per}), as given by Eq. (9) and Eq. (10), respectively.

$$\delta\Delta t^{\text{con}}(a_0) = +\frac{3}{2}\frac{GM(a_0 - a_n)}{(a_0 c)^2}, \tag{9}$$

$$\delta\Delta t^{\text{rel}} = \frac{a_E^2}{2a^2c^2} J_2 \left[3\sqrt{GMa}\sin^2 i \sin 2u - 7\frac{GM}{a}\left(1 - \frac{3}{2}\sin^2 i\right) t\right], \tag{10}$$

where GM is the product of the gravitational constant and the Earth's mass, a is the semimajor axis, J_2 is the gravity term, a_E is the semimajor axis of the Earth, i is the orbit inclination, and u is the argument of latitude.

3. Results and discussions

The variations in the clock corrections of the 12 operational GPS Block IIF satellites were analyzed, where satellite clocks with standard deviations (SDs) smaller than first quantile of SDs would be selected for this study. Three satellite clocks met this criterion, as described in Table 2. The clocks were labeled with the pseudo-random noise (PRN) [30] (i.e., PG01, PG10 and PG30), which is the code of the satellite that carries the clock. We obtained 6,640 days of data from the three GPS Block IIF satellites, spanning 23 March 2014 to 25 July 2020. Fig. 2 shows the raw clock correction for each clock. Outliers were removed if they were typically more than 3σ, which represented 2.1% for PG01, 7.3% for PG10, and less than 1.0% for PG30 of the data. The data were corrected for the relativistic corrections and systematic effects. The change in the clock correction linear fit slopes against the estimated radial distance, as shown in Fig. 1, represents a linear fit for the period number 2008 (12:00:00 UTC, 20 December 2016) for PG01, as an example of linear fit. To remove the annual oscillation and short-term fluctuations, the data were split by year and then smoothed with a 16-day moving average. The moving average window was chosen based on the frequency distribution of the Fourier analysis.

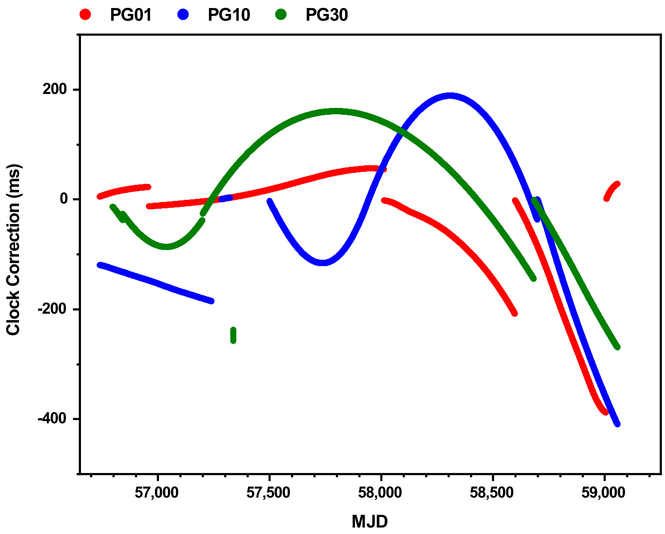

Fig. 2. Raw clock corrections generated by GFZ. Y-axis represents raw clock corrections in milliseconds, and X-axis shows Modified Julian Days (MJD).

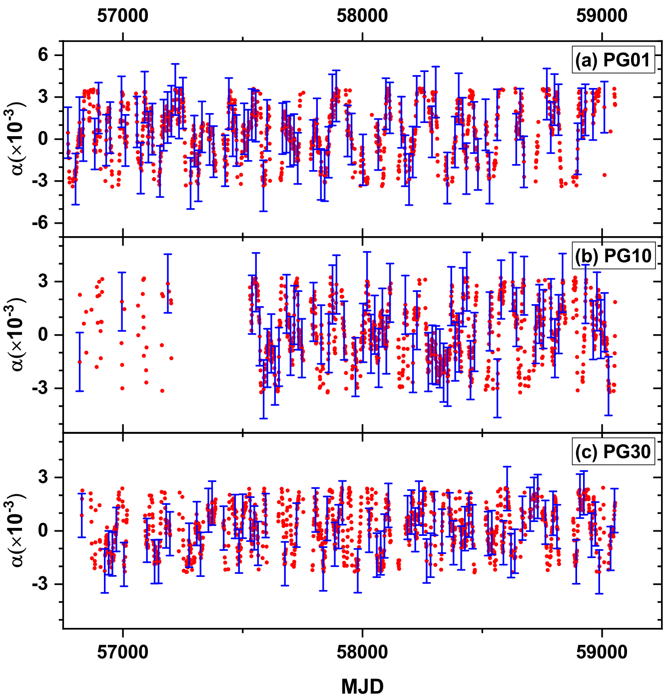

Fig. 3. Distribution of daily test parameter α results for (a) PG01, (b) PG10, and (c) PG30. Error bars indicate 1σ fit errors from respective least-squares fit.

Eq. (5) was utilized to fit the data, then the annual oscillation, i.e., $B\cos\left(\frac{2\pi t}{T_d}+\varphi\right)$, was subtracted from the daily values. The data were more sensitive to annual oscillation than short-term fluctuations.

Table 1 shows the results derived from the distribution of fitted test parameters α for the three Rb clocks. Some bias in the distribution of all three clocks could be observed, which indicated that some systematic effects still remained in our data. This occurred because we addressed only temperature, magnetic field errors, and SRP correction of orbital uncertainty. The LPI violations found from PG01, PG10, and PG30 are $(0.49 \pm 1.85) \times 10^{-3}$, $(0.14 \pm 1.67) \times 10^{-3}$, and $(0.17 \pm 1.26) \times 10^{-3}$, respectively. Compared with the first test of LPI violation using RAFS, which indicated that the boundary is $-0.0027 < \beta_f < 0.0030$ [12], our results improve the LPI violation by factors of 1.6, 1.8, and 2.4, respectively. The distributions of the daily test parameter α for PG01, PG10, and PG30 are shown in Fig. 3.

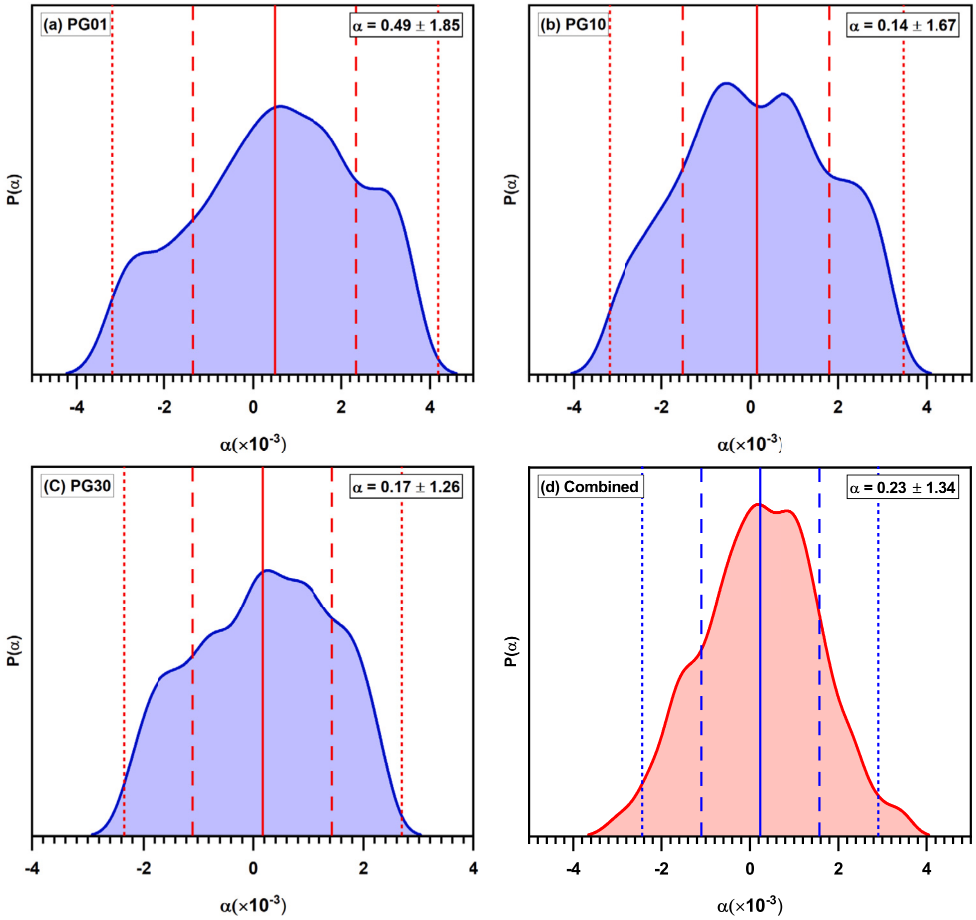

Fig. 4. Test parameter α including systematic corrections for each clock as well as for combination of all three clocks, as shown in panel (a) PG01, (b) PG10, (c) PG30 and (d) Combined, respectively. Vertical lines mark mean (solid lines) as well as equal-tailed 68% (dashed lines) and 95% (dotted lines) confidence intervals.

The final results were obtained by combining all clocks (equal weights were assigned to all clocks), and the limit was $(0.23 \pm 1.34) \times 10^{-3}$, which improved the [12] by a factor of 2.2. The probability distributions of the test parameter α for each clocks and their combination are shown in Fig. 4.

The accuracy of testing the LPI parameters crucially depends on the accuracy of the clock, and for this test, long-term stability in the orbital period term or longer is appropriate [31]. Long-term clock stability limits depend on frequency biases that can vary in time in respond to external or operational parameters acting upon the AFS [32]. Because of its higher frequency stability and lower drift, PHM is more accurate than RAFS [18,33–36]. This higher accuracy makes PHM the perfect tool for testing the fundamental law of physics, which is why H masers were used in space for the first time [37]. However, because of the lack of necessary information, systematic errors for GPS clocks have not been completely modeled. Therefore, some uncounted systematic errors still remain in the data, which prevents improvements in gravitational redshift tests using GPS IIF RAFS. The main advantages of RAFS are its small volume, low cost, and low power consumption compared with those of other AFSs, so RAFS is the most-used AFS in space applications [32]. Improvements in the modeling or measurement of the clock environment, using a clock with higher stability, and reducing the effect of orbit determination can substantially improve tests for future experiments.

4. Conclusions

Since 1976, the GPA mission has been the most accurate test for gravitational redshift, which uses comparisons of hydrogen masers at heights of 10,000 km above the ground with its ground-based counterpart. The latest improvement to the GPA test was presented in 2018 [10,11] using about three years of data from three PHM clocks, producing improvement factors of 5.6 and 4.0. GPS atomic clocks were used to test LPI in 2012 [12] using Rb clocks on board GPS satellites. This study analyzed 6,640 days of data from three stable Rb clocks on board GPS Block IIF satellites with more eccentric orbits. The systemic effects that we considered included temperature and magnetic field errors, SRP correction in orbital modeling error, and the improved relativistic correction. However, the orbit radial errors were unable to be removed because the SLR data were unavailable for GPS IIF satellites. The fractional deviation of the gravitational redshift from the general relativity prediction estimated by the combination of these three Rb clocks is $(0.23 \pm 1.34) \times 10^{-3}$. In addition to the improvements in atomic clock technology in recent years, we improved the statistics and considered the possible systematic errors, which improved the limit of LPI violation presented by [12] by a factor of 2.2.

Optical atomic clock is a new kind of clock with the ability to measure time based on optical frequency standards. These clocks use trapped ions and many neutral atoms with fractional frequency uncertainties of 1 part in 10^{18} [38–42]. The development of stabilized femtosecond-laser frequency combs and improvements in laser cooling/trapping techniques in cooperation with advances in atomic quantum systems has led to rapid improvements in clocks at optical frequencies [43,44]. Using optical atomic clocks will improve the uncertainty for α to 1×10^{-9} [45]. The ability to directly measure the environmental parameters of clocks [45], improvements in clock technology [46], and available SLR corrections for new generations of GNSS satellites, thereby lead to new studies to considerably improve the test in the future.

CRediT authorship contribution statement

- Loghman Fathollahi: Conceived and designed the experiments; Performed the experiments; Analyzed and interpreted the data; Contributed reagents, materials, analysis tools and data; Wrote the paper.
- Falin Wu: Conceived and designed the experiments; Analyzed and interpreted the data; Wrote the paper.
- Barbara Pongracic: Analyzed and interpreted the data; Contributed reagents, materials, analysis tools and data; Wrote the paper.

Declaration of competing interest

The authors declare no competing interests.

Data availability

Data included in article/supplementary material/referenced in article.

Funding statement

This research did not receive any specific grant from funding agencies in public, commercial, or no-for-profit sectors.

Additional information

No additional information is available for this paper.

References

[1] V.A. Kostelecký, J.D. Tasson, Matter-gravity couplings and Lorentz violation, Phys. Rev. D 83 (2011) 016013, https://doi.org/10.1103/PhysRevD.83.016013.
[2] C.M. Will, The confrontation between general relativity and experiment, Living Rev. Relativ. 17 (14) (2014) 4–117, https://doi.org/10.12942/lrr-2014-4.
[3] A. Godone, C. Novero, P. Tavella, Null gravitational redshift experiment with nonidentical atomic clocks, Phys. Rev. D 51 (1995) 319–323, https://doi.org/10.1103/PhysRevD.51.319.
[4] M.A. Hohensee, S. Chu, A. Peters, H. Müller, Equivalence principle and gravitational redshift, Phys. Rev. Lett. 106 (2011) 151102, https://doi.org/10.1103/PhysRevLett.106.151102.
[5] R.V. Pound, G.A. Rebka, Apparent weight of photons, Phys. Rev. Lett. 4 (1960) 337–341, https://doi.org/10.1103/PhysRevLett.4.337.
[6] R.V. Pound, J.L. Snider, Effect of gravity on nuclear resonance, Phys. Rev. Lett. 13 (1964) 539–540, https://doi.org/10.1103/PhysRevLett.13.539.
[7] R.F.C. Vessot, M.W.A. Levine, A test of the equivalence principle using a space-borne clock, Gen. Relativ. Gravit. 10 (1979) 181–204, https://doi.org/10.1007/BF00759854.
[8] R.F.C. Vessot, M.W. Levine, E.M. Mattison, E.L. Blomberg, T.E. Hoffman, G.U. Nystrom, B.F. Farrel, R. Decher, P.B. Eby, C.R. Baugher, J.W. Watts, D.L. Teuber, F.D. Wills, Test of relativistic gravitation with a space-borne hydrogen maser, Phys. Rev. Lett. 45 (1980) 2081–2084, https://doi.org/10.1103/PhysRevLett.45.2081.
[9] R.F.C. Vessot, Clocks and spaceborne tests of relativistic gravitation, Adv. Space Res. 9 (9) (1989) 21–28, https://doi.org/10.1016/0273-1177(89)90004-5.
[10] P. Delva, N. Puchades, E. Schönemann, C.C.F. Dilssner, S. Bertone, A.H.F. Gonzalez, C.L. Poncin-Lafitte, F. Meynadier, R. Prieto-Cerdeira, B. Sohet, J. Ventura-Traveset, P. Wolf, Gravitational redshift test using eccentric Galileo satellites, Phys. Rev. Lett. 121 (2018) 231101, https://doi.org/10.1103/PhysRevLett.121.231101.
[11] S. Herrmann, F. Finke, M. Lülf, O. Kichakova, D. Puetzfeld, D. Knickmann, M. List, B. Rievers, G. Giorgi, C. Günther, H. Dittus, R. Prieto-Cerdeira, F. Dilssner, F. Gonzalez, E. Schönemann, J. Ventura-Traveset, C. Lämmerzahl, Test of the gravitational redshift with Galileo satellites in an eccentric orbit, Phys. Rev. Lett. 121 (2018) 231102, https://doi.org/10.1103/PhysRevLett.121.231102.
[12] J. Kentosh, M. Mohageg, Global positioning system test of the local position invariance of Planck's constant, Phys. Rev. Lett. 108 (2012) 110801, https://doi.org/10.1103/PhysRevLett.108.110801.
[13] International GNSS Service (IGS), the International GNSS Service (IGS) products, available from: http://www.igs.org/products, 2020.
[14] The Global Positioning System (GPS), GPS space segment, available from: https://www.gps.gov/systems/gps/space/, 2020.
[15] Boeing, Boeing space, global positioning system IIF, available from: http://www.boeing.com/space/global-positioning-system/, 2020.
[16] R.T. Dupuis, T.J. Lynch, J.R. Vaccaro, Rubidium frequency standard for the GPS IIF program and modifications for the RAFSMOD program, in: Proceedings of the IEEE International Frequency Control Symposium, American Statistical Association, Honolulu, HI, USA, 2008, pp. 655–660.
[17] F. Droz, P. Mosset, G. Barmaverain, P. Rochat, Q. Wang, M. Belloni, L. Mattioni, U. Schmidt, T. Pike, F. Emma, P. Waller, The on-board Galileo clocks: rubidium standard and passive hydrogen maser - current status and performance, in: Proceedings of the 20th European Frequency and Time Forum, Braunschweig, Germany, 2006, pp. 420–426.

[18] F. Vannicola, R. Beard, D. Koch, A. Kubik, D. Wilson, J. White, GPS block IIF atomic frequency standard analysis, in: Proceedings of the 45th Annual Precise Time and Time Interval Systems and Applications Meeting, Bellevue, Washington, USA, 2013, pp. 244–249.

[19] N. Ashby, Relativity in the global positioning system, Living Rev. Relativ. 6 (2003) 1–42, https://doi.org/10.12942/lrr-2003-1.

[20] P. Delva, A. Hees, S. Bertone, E. Richard, P. Wolf, Test of the gravitational redshift with stable clocks in eccentric orbits: application to Galileo satellites 5 and 6, Class. Quantum Gravity 32 (23) (2015) 232003, https://doi.org/10.1088/0264-9381/32/23/232003.

[21] V. Angelopoulos, D. Sibeck, C.W. Carlson, J.P. McFadden, D. Larson, R.P. Lin, J.W. Bonnell, F.S. Mozer, R. Ergun, C. Cully, K.H. Glassmeier, U. Auster, A. Roux, O. LeContel, S. Frey, T. Phan, S. Mende, H. Frey, E. Donovan, C.T. Russell, R. Strangeway, J. Liu, I. Mann, J. Rae, J. Raeder, X. Li, W. Liu, H.J. Singer, V.A. Sergeev, S. Apatenkov, G. Parks, M. Fillingim, J. Sigwarth, First results from the THEMIS mission, Space Sci. Rev. 141 (2008) 453–476, https://doi.org/10.1007/s11214-008-9378-4.

[22] N.A. Tsyganenko, M.I. Sitnov, Magnetospheric configurations from a high-resolution data-based magnetic field model, J. Geophys. Res. Space Phys. 112 (2007) 148–227, https://doi.org/10.1029/2007JA012260.

[23] E. Thébault, C.C. Finlay, C.D. Beggan, P. Alken, J. Aubert, O. Barrois, F. Bertrand, T. Bondar, A. Boness, L. Brocco, E. Canet, A. Chambodut, A. Chulliat, P. Coïsson, F. Civet, A. Du, A. Fournier, I. Fratter, N. Gillet, B. Hamilton, M. Hamoudi, G. Hulot, T. Jager, M. Korte, W. Kuang, X. Lalanne, B. Langlais, J.-M. Léger, V. Lesur, F.J. Lowes, S. Macmillan, M. Mandea, C. Manoj, S. Maus, N. Olsen, V. Petrov, V. Ridley, M. Rother, T.J. Sabaka, D. Saturnino, R. Schachtschneider, O. Sirol, A. Tangborn, A. Thomson, L. Tøffner-Clausen, P. Vigneron, I. Wardinski, T. Zvereva, International geomagnetic reference field: the 12th generation, Earth Planets Space 67 (2015) 79, https://doi.org/10.1186/s40623-015-0228-9.

[24] A. Wu, Performance evaluation of the GPS block IIR time keeping system, in: Proceedings of the 28th Annual Precise Time and Time Interval Systems and Applications Meeting, Reston, Virginia, USA, 1996, pp. 441–454.

[25] O. Montenbruck, P. Steigenberger, U. Hugentobler, Enhanced solar radiation pressure modeling for Galileo satellites, J. Geod. 89 (2015) 283–297, https://doi.org/10.1007/s00190-014-0774-0.

[26] B. Duan, U. Hugentobler, Enhanced solar radiation pressure model for GPS satellites considering various physical effects, GPS Solut. 25 (2021) 42, https://doi.org/10.1007/s10291-020-01073-z.

[27] German Research Centre for geosciences (GFZ), GFZ analysis center notes, available from: ftp://ftp.igs.org/pub/center/analysis/gfz.acn, 2020.

[28] J. Kouba, Improved relativistic transformations in GPS, GPS Solut. 8 (2004) 170–180, https://doi.org/10.1007/s10291-004-0102-x.

[29] G. Petit, B. Luzum, IERS conventions (2010), IERS Technical Note 36, Bureau International des Poids et Mesures (BIPM), and US Naval Observatory (USNO), Frankfurt Am Main, 2010.

[30] B.W. Parkinson, J.J. Spilker, P. Axelrad, P. Enge, Global Positioning System: Theory and Applications, American Institute of Aeronautics and Astronautics, Washington, DC, USA, 1996.

[31] N. Ashby, T.E. Parker, B.R. Patla, A null test of general relativity based on a long-term comparison of atomic transition frequencies, Nat. Phys. 14 (2018) 822–826, https://doi.org/10.1038/s41567-018-0156-2.

[32] E. Batori, N. Almat, C. Affolderbach, G. Mileti, GNSS-grade space atomic frequency standards: current status and ongoing developments, Adv. Space Res. 68 (12) (2021) 4723–4733, https://doi.org/10.1016/j.asr.2020.09.012.

[33] P. Rochat, F. Droz, P. Mosset, G. Barmaverain, Q. Wang, D. Boving, L. Mattioni, M. Belloni, M. Gioia, U. Schmidt, T. Pike, F. Emma, The onboard Galileo rubidium and passive maser, status & performance, in: Proceedings of the 2005 IEEE International Frequency Control Symposium and Exposition, Vancouver, BC, Canada, 2005, pp. 26–32.

[34] L. Lorini, N. Ashby, A. Brusch, S. Diddams, R. Drullinger, E. Eason, T. Fortier, P. Hastings, T. Heavner, D. Hume, W. Itano, S. Jefferts, N. Newbury, T. Parker, T. Rosenband, J. Stalnaker, W. Swann, D. Wineland, J. Bergquist, Recent atomic clock comparisons at NIST, Eur. Phys. J. Spec. Top. 163 (1) (2008) 19–35, https://doi.org/10.1140/epjst/e2008-00807-7.

[35] A. Hauschild, O. Montenbruck, P. Steigenberger, Short-term analysis of GNSS clocks, GPS Solut. 17 (2013) 295–307, https://doi.org/10.1007/s10291-012-0278-4.

[36] P. Zhang, R. Tu, Y. Gao, J. Hong, J. Han, X. Lu, Comparison of multi-GNSS time and frequency transfer performance using overlap-frequency observations, Remote Sens. 13 (16) (2021) 3130, https://doi.org/10.3390/rs13163130.

[37] N. Bhaskar, J. White, L. Mallette, T. McClelland, J. Hardy, A historical review of atomic frequency standards used in space systems, in: Proceedings of 1996 IEEE International Frequency Control Symposium, Vancouver, BC, Canada, 1996, pp. 24–32.

[38] R.M. Godun, P.B.R. Nisbet-Jones, J.M. Jones, S.A. King, L.A.M. Johnson, H.S. Margolis, K. Szymaniec, S.N. Lea, K. Bongs, P. Gill, Frequency ratio of two optical clock transitions in $^{171}\mathrm{yb}^{+}$ and constraints on the time variation of fundamental constants, Phys. Rev. Lett. 113 (2014) 210801, https://doi.org/10.1103/PhysRevLett.113.210801.

[39] N. Huntemann, C. Sanner, B. Lipphardt, C. Tamm, E. Peik, Single-ion atomic clock with 3×10^{-18} systematic uncertainty, Phys. Rev. Lett. 116 (2016) 063001, https://doi.org/10.1103/PhysRevLett.116.063001.

[40] W.F. McGrew, X. Zhang, R.J. Fasano, S.A. Schäffer, K. Beloy, D. Nicolodi, R.C. Brown, N. Hinkley, G. Milani, M. Schioppo, T.H. Yoon, A.D. Ludlow, Atomic clock performance enabling geodesy below the centimetre level, Nature 564 (2018), https://doi.org/10.1038/s41586-018-0738-2.

[41] T. Bothwell, D. Kedar, E. Oelker, J.M. Robinson, S.L. Bromley, W.L. Tew, J. Ye, C.J. Kennedy, JILA SrI optical lattice clock with uncertainty of 2.0×10^{-18}, Metrologia 56 (6) (2019) 065004, https://doi.org/10.1088/1681-7575/ab4089.

[42] S.M. Brewer, J.-S. Chen, A.M. Hankin, E.R. Clements, C.W. Chou, D.J. Wineland, D.B. Hume, D.R. Leibrandt, $^{27}\mathrm{al}^{+}$ quantum-logic clock with a systematic uncertainty below 10^{-18}, Phys. Rev. Lett. 123 (2019) 033201, https://doi.org/10.1103/PhysRevLett.123.033201.

[43] A.D. Ludlow, M.M. Boyd, J. Ye, E. Peik, P.O. Schmidt, Optical atomic clocks, Rev. Mod. Phys. 87 (2015) 637–701, https://doi.org/10.1103/RevModPhys.87.637.

[44] C. Sanner, N. Huntemann, R. Lange, C. Tamm, E. Peik, M.S. Safronova, S.G. Porsev, Optical clock comparison for Lorentz symmetry testing, Nature 567 (2019) 204–208, https://doi.org/10.1038/s41586-019-0972-2.

[45] A. Derevianko, K. Gibble, L. Hollberg, N.R. Newbury, C. Oates, M.S. Safronova, L.C. Sinclair, N. Yu, Fundamental physics with a state-of-the-art optical clock in space, Quantum Sci. Technol. 7 (4) (2022) 044002, https://doi.org/10.1088/2058-9565/ac7df9.

[46] T. Bothwell, C.J. Kennedy, A. Aeppli, D. Kedar, J.M. Robinson, E. Oelker, A. Staron, J. Ye, Resolving the gravitational redshift across a millimetre-scale atomic sample, Nature 602 (7897) (2022) 420–424, https://doi.org/10.1038/s41586-021-04349-7.